

PAPER • OPEN ACCESS

Electron impact resonances of uracil in an aqueous environment from anion photoelectron imaging

To cite this article: Graham A Cooper *et al* 2023 *J. Phys. B: At. Mol. Opt. Phys.* **56** 185102

View the [article online](#) for updates and enhancements.

You may also like

- [Interactions between low energy electrons and DNA: a perspective from first-principles simulations](#)
Jorge Kohanoff, Maeve McAllister, Gareth A Tribello *et al.*
- [Meteorites and the RNA World: Synthesis of Nucleobases in Carbonaceous Planetesimals and the Role of Initial Volatile Content](#)
Klaus Paschek, Dmitry A. Semenov, Ben K. D. Pearce *et al.*
- [Molecular dynamics simulations disclose early stages of the photo-activation of cryptochrome 4](#)
Daniel R Kattnig, Claus Nielsen and Ilia A Solov'yov

Electron impact resonances of uracil in an aqueous environment from anion photoelectron imaging

Graham A Cooper, Connor J Clarke  and Jan R R Verlet* 

Department of Chemistry, Durham University, Durham DH1 3LE, United Kingdom

E-mail: j.r.r.verlet@durham.ac.uk

Received 2 June 2023, revised 4 August 2023

Accepted for publication 23 August 2023

Published 7 September 2023



CrossMark

Abstract

The effect that solvation has on electron attachment to uracil, U, was studied by probing the electronic resonances of the uracil radical anion, U^- , in gas-phase water clusters, $U^-(H_2O)_n$, using photoelectron imaging across a range of photon energies. Specifically, the π_3^* shape resonance was probed in detail and the spectral signatures following excitation to this resonance are considered. Several new methods for analysis are provided to capture the different actions of the resonance on the photoelectron emission, which in turn provide insight into the location of the π_3^* resonance and its subsequent dynamics. The effect of solvation on each action observed through the photoelectron emission is studied for $n \leq 10$. We find that the actions—be they related to statistical emission, prompt autodetachment, or the photoelectron angular distributions—all become less sensitive as the cluster size increases, suggesting that their use for very large clusters may be limited. Additionally, we consider the correlation between electron detachment from the anion, as probed in the experiments, and electron attachment to the neutral. Specifically, they are linked through the reorganisation energy in a linear response picture and we show how the cluster approach developed here allows one to decompose the total reorganisation energy into intramolecular (associated with the anion to neutral geometry change in U) and intermolecular (associated with the change in hydration sphere) contributions. For U in a bulk aqueous environment, we find that the total reorganisation energy, $\lambda \sim 1.2$ eV, shows equal contributions from both intra- and intermolecular changes.

Keywords: electron impact, resonances, uracil, aqueous, anion

(Some figures may appear in colour only in the online journal)

1. Introduction

When high-energy radiation passes through aqueous materials, including living cells, secondary electrons are produced in large quantities with mean energies around <10 eV [1–3].

These secondary low-energy electrons can induce chemical changes with important consequences [1, 4–6]. For example, Sanche and coworkers showed that low-energy electrons can lead to single- and double-strand breaks in DNA [7, 8]. These experiments clearly show that the chemical processes occur at specific energies, thus implying that electronic resonances are responsible for the initial capture to form temporary negative ions that lead to reaction. In the case of DNA, one accepted mechanism for DNA damage involves the initial capture of the electron through the π^* shape resonances of the nucleobases, which then connects non-adiabatically to a σ^* state that ruptures the sugar-phosphate C–O bond [9]. Probing such a

* Author to whom any correspondence should be addressed.



Original content from this work may be used under the terms of the [Creative Commons Attribution 4.0 licence](https://creativecommons.org/licenses/by/4.0/). Any further distribution of this work must maintain attribution to the author(s) and the title of the work, journal citation and DOI.

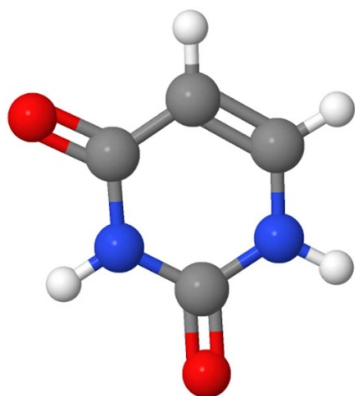


Figure 1. Structure of uracil: carbon (dark grey), nitrogen (blue), oxygen (red), hydrogen (white).

process experimentally has not been feasible to date, although much effort has gone into understanding the initial resonances that are available for the electron capture. To this end, the π^* shape resonances of the nucleobases have been studied by electron transmission spectroscopy, which provide the energetic positions of the resonances; and by ion yield spectroscopy, which probes any dissociative electron attachment processes that may be taking place [10–16]. These experiments have been performed on the targets in isolation (gas-phase). In contrast, experimental studies extending this to more complex environments such as water have been scarce. Kočišek *et al* performed elegant experiments on uracil (U, the structure of which is shown in figure 1) and thymine (T) water clusters, $U(H_2O)_n$ and $T(H_2O)_n$, subjected to electrons with energies below 3 eV [17]. They found that the dissociative electron attachment channel that is present for U and T was suppressed in $U(H_2O)_n$ and $T(H_2O)_n$ by the observation of the intact parent anion. However, the initial nucleobase-water clusters are not mass-selected in their experiments so it is non-trivial to relate the findings to specific cluster sizes or resonances. Approaching dynamics from the bulk is also non-trivial. Electron scattering means that the initial energy cannot be defined and free electrons rapidly form hydrated electrons, which are bound.

We have recently developed a less conventional approach to probing electron-impact resonances by using anion photoelectron imaging [18–21]. Starting from the ground-state anion, light can access specific excited states of the anion that are buried in the continuum. In principle, these are the same states as the electron-impact resonances probed in electron scattering experiments. While selection rules for electron-excitation and photon-excitation are different, at the energies considered here, both follow the dipole-approximation and are therefore comparable to some extent, especially when only considering resonance locations rather than cross sections, as considered in the present work. The main downside is that the initial geometries of the anion and neutral can differ so that direct comparison between the two can be skewed unless the structures are similar. On the other hand, the substantial benefits are that (i)

light offers a means of introducing time-resolution in a trivial manner through time-resolved photoelectron spectroscopy [22–24] and (ii) because the target is charged, it can be mass-selected prior to the interaction with light [19]. The latter allows one to separate clusters with a chosen number of solvent molecules and therefore provides a path into experimentally probing electronic resonances in mass-selected solute-solvent clusters [25–27]. We have recently applied this technique to probe the resonances in $U^-(H_2O)_n$ [28]. Here, we expand on this work by demonstrating how resonances can be identified through various spectroscopic observables, and how the intrinsic geometry changes between anion and neutral for the solute can be unpicked from the solvent interactions, which underpin the total reorganisation energy in the electron loss or gain process [29, 30]. This is essential to link vertical excitation energies from anions to vertical electron attachment energies by the corresponding neutral molecule.

This paper is organised as follows. Section 2 describes the methodology used with results and analysis of those offered in section 3. Section 3 is divided into subsections: first presenting the 2D photoelectron spectra, followed by examining different observables of the resonance position of U in the water clusters with discussion of their merits and demerits. Section 4 considers the evolution of observables for larger clusters and how these extrapolate to the bulk limit, and also provides a breakdown of the total reorganisation energy in terms of intra- and inter-molecular contributions. Section 5 closes with the key conclusions.

2. Methodology

The experiment has an anion source, a time-of-flight mass spectrometer [31] to separate anions, and a velocity map imaging spectrometer [32, 33] to measure photoelectron images and spectra of mass-selected anions. The experiment has been described in detail previously [34] and only a brief outline is provided here. A sample of solid U (Sigma Aldrich, $\geq 99\%$) was heated to a temperature of 230 °C in an Even-Lavie valve [35]. Water was provided by adding a drop of water in the backing gas line. Nitrogen gas at ~ 5 –6 bar was used as a backing gas and co-expanded with the vapour pressure of U and H_2O into vacuum. Radical anions, U^- , were produced using a ring-filament ionizer that injected electrons into the supersonic expansion, predominantly producing a distribution of $U^-(H_2O)_n$. The expansion entered a Wiley–McLaren time-of-flight mass spectrometer [31], which separates anions by the mass-to-charge ratio. Packets of mass-selected ions were intersected at the focal point of the mass spectrometer with light from a Nd:YAG pumped optical parametric oscillator (Continuum, Horizon). The electrons produced were collected using a velocity map imaging photoelectron spectrometer [34]. The images were reconstructed using polar onion peeling and calibrated using iodide [36]. The resultant energy resolution was on the order of 5% of the photoelectron’s kinetic energy.

3. Results and analysis of resonance positions

3.1. 2D photoelectron spectra

A representative 2D photoelectron spectrum is shown in figure 2(a) for $\text{U}^-(\text{H}_2\text{O})_2$ over a photon energy range of $1.2 \leq h\nu \leq 5.2$ eV. The 2D photoelectron spectra for $n = 3, 4, 6, 8,$ and 10 are broadly similar [28]. The main features are as follows. There are two diagonal features, one starting at $h\nu \sim 1.5$ eV and a second at $h\nu \sim 4.6$ eV. Diagonal features are generally associated with a prompt detachment channel in which, by the photoelectric effect, the electron kinetic energy (eKE) increases by an amount equal to the increase in $h\nu$ [19]. Of these two features, the one appearing at lower photon energy corresponds to the direct detachment of the open-shell anion to the neutral ground state (S_0), while the higher energy feature leaves the neutral in an excited state (T_1). The ground state of $\text{U}^-(\text{H}_2\text{O})_{n > 1}$ is a valence state in which the excess electron occupies the π_1^* resonance of the bare U^- , which has become bound by the strong anion-dipole interaction within the cluster [37, 38].

In addition to these direct detachment features, there is clear evidence of resonances being accessed. These can appear in the 2D photoelectron spectra in several ways. First, the appearance of electron emission peaking at eKE = 0 eV with a Boltzmann distribution is direct evidence of the formation of a bound state from which electrons are lost statistically (i.e. leading to the Boltzmann distribution). Statistical (or thermionic) emission typically occurs on a timescale of many nanoseconds to microseconds and even milliseconds (depending on the number of internal modes and the electron affinity of the species), which implies that electron emission is taking place from the electronic ground state of the anion [39–41] (although excited state emission has been observed too [42]). The appearance of statistical emission is therefore a clear indicator of resonances being populated that then decay to reform the anion ground state [19]. In figure 2(a), such emission is evident for $h\nu < 3$ eV and around $h\nu = 3.9$ eV. These two regions correspond to excitation to the π_2^* and π_3^* resonances of U^- , respectively [28].

A second signature of the population of electronic resonances is changes in the photoelectron spectrum compared to direct detachment [19]. Specifically, upon excitation of a resonance, both the differing Franck–Condon factors and resonance dynamics can lead to variations in the photoelectron spectrum. Such features were particularly apparent in the 2D photoelectron spectra of polycyclic aromatic hydrocarbon radical anions [20, 21, 43]. In figure 2(a), around $h\nu = 3.9$ eV, the peak at high eKE (around 2 eV) clearly shifts towards lower eKE relative to the expected position from the linear trend otherwise observed. Additionally, some photoelectron signal can be seen between this feature and the statistical emission peak, indicating that electrons are being emitted along some nuclear coordinates which are bringing the resonance closer in energy to the neutral ground state (as commonly observed in 2D electron energy loss spectra [44, 45]). Such evidence of nonadiabatic dynamics is consistent with the ultimate appearance of statistical emission arising from the bound anion ground state.

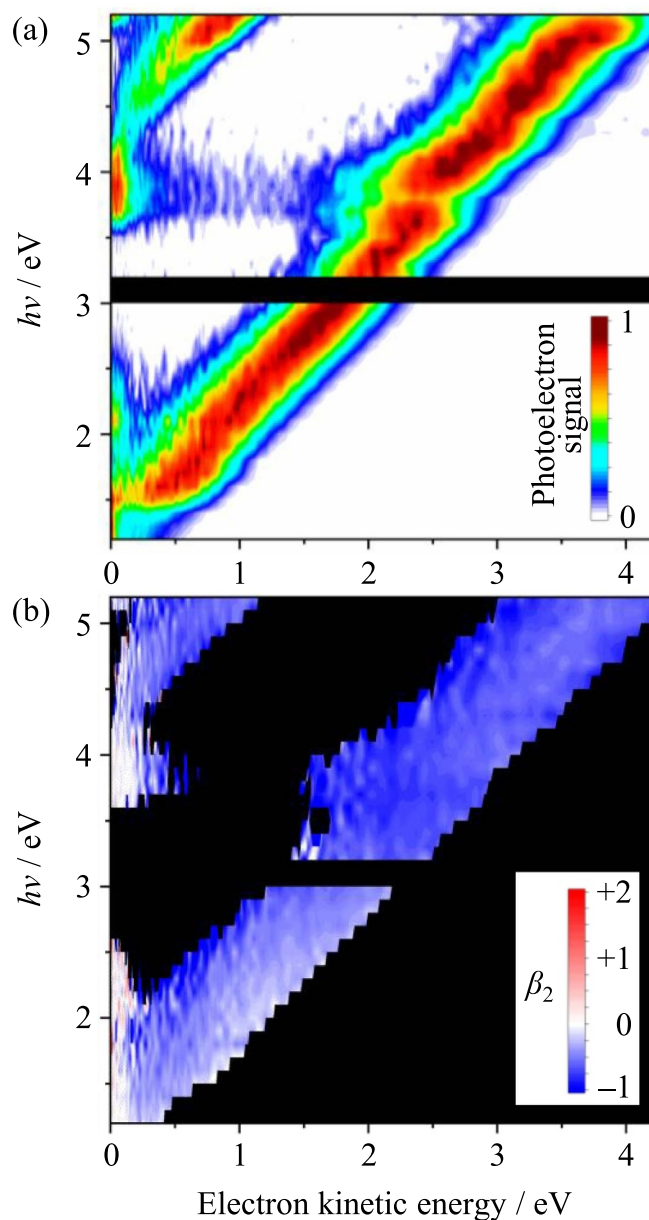


Figure 2. (a) 2D photoelectron spectrum of $\text{U}^-(\text{H}_2\text{O})_2$ in the photon energy ($h\nu$) range from 1.2 to 5.2 eV, adapted from [28]. (b) Corresponding photoelectron anisotropy parameters. Black shaded areas indicate no meaningful signal. In (a), no photoelectron spectrum was acquired at $h\nu = 3.1$ eV and additionally in (b), angular distributions for photoelectron signals less than 10% of the maximum have been omitted.

Finally, a third signature of resonances being excited can be gleaned from the photoelectron angular distributions [46, 47]. Figure 2(b) shows photoelectron angular distributions as a 2D map corresponding to the 2D photoelectron spectrum, quantified by the anisotropy parameter, β_2 , which has limiting values of +2 and -1 [48]. For photoelectron emission predominantly parallel to the laser polarisation axis, $\beta_2 = +2$, while if the emission is predominantly perpendicular to the laser polarisation axis, $\beta_2 = -1$. Qualitatively, β_2 is sensitive to the orbital from which the electron has been emitted [46, 47]. For direct detachment, β_2 is generally a slowly varying function with

eKE (or $h\nu$ in the present case), because the photodetachment cross-sections for the various partial waves and their relative phases are slowly varying functions of energy. Hence, when a resonance is excited and an electron is lost from a resonance, it is possible that the β_2 associated with that emission changes abruptly as $h\nu$ is scanned, reflecting changes in the character of the molecular orbital from which the electron is emitted [18–21]. Such changes are visible in figure 2(b) around $h\nu = 3.9$ eV and discussed further below.

In the next three sub-sections, we use the above observations to obtain ‘spectral’ signatures for resonances observed in $U^-(H_2O)_n$, focussing on the π_3^* resonance around $h\nu = 3.9$ eV. For each method, we explain the limitation of using the specific observable in determining resonance positions, which pertains particularly to water clusters.

3.2. Ratio of direct to indirect detachment

The first method to determine the resonance location exploits the observation of statistical emission, which has been applied previously both in isolated [18, 23, 49, 50] and clustered anions [23, 51, 52]. As mentioned, the appearance of such emission implies that the ground state is repopulated. For the case of the π_3^* resonance around $h\nu \sim 3.9$ eV (figure 2), this implies that initial excitation to the resonance from the π_1^* bound state will lead somehow to internal conversion back to the π_1^* state, either directly or via a lower-lying electronic state or resonance (e.g. the π_2^* state/resonance). Regardless of the mechanism, the statistical emission can only occur when the π_3^* resonance is initially excited and, hence, is an indirect measure of its presence. Figure 3 shows a photoelectron spectrum for $U^-(H_2O)_2$ taken at $h\nu = 3.9$ eV, corresponding to a slice through figure 2(a) at $h\nu = 3.9$ eV. The peak associated with the direct detachment is clearly seen at eKE ~ 2 eV and the statistical emission peaking at eKE = 0 eV. To obtain an action spectrum associated with the π_3^* resonance, one can therefore take a ratio of the signal associated with the statistical detachment to the signal associated with the direct detachment. There are a number of ways in which that ratio can be determined. The ratio can be taken as peak amplitudes, integrated signals over spectral ranges, or by fitting the signals to representative functions and using these to obtain suitable ratios. Each variation was found to offer very similar results.

Figure 4 shows the ratio determined by fitting the statistical photoelectron feature to an exponentially decaying function, and the prompt photoelectron signal to a Gaussian function. The ratio shows a peak when the photon energy crosses the π_3^* resonance as the photoexcited resonance decays to the ground electronic state producing enhanced statistical emission. The overall contrast is very good and remains reasonably good even for larger clusters (up to $n = 10$). However, the absolute ratio (not shown in figure 4) has decreased by about an order of magnitude for $n = 10$ compared to $n \leq 6$, suggesting that there will be a limit to how far this method can be extended to much larger clusters.

Like all action spectroscopic methods, the limitation of the method lies in the action that is observed. In the present case, we focus on electron emission as the observable. The timescale

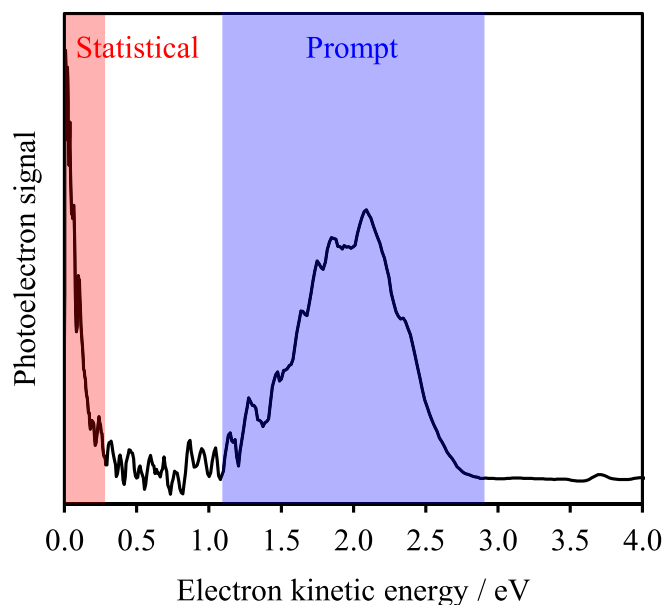


Figure 3. Photoelectron spectrum of $U^-(H_2O)_2$ taken at $h\nu = 3.9$ eV. Red and blue shaded areas indicate statistical and prompt photoelectron signal, respectively.

over which emission is measured in the current experiments is ~ 200 ns (timescale over which the extractor plate in the imaging spectrometer was pulsed), which means that any emission that is slower, or any processes that do not lead to emission at all, will not be captured. In the case of $U^-(H_2O)_n$, reformation of the ground state following excitation of the π_3^* resonance will lead not only to electron loss as a possible statistical decay process, but also evaporation. Both will be in competition and which will dominate depends on factors such as the water binding energies in the clusters and the electron affinity. As the clusters become larger, the electron affinity increases and the binding energy per water molecule decreases [53] such that we might expect evaporation to become more dominant at larger n . Indeed, we know evaporation can happen as this was the action used by Kočišek *et al* in their experiment probing $U^-(H_2O)_m$ formation upon electron attachment to $U^-(H_2O)_n$, where $m < n$ [17]. It also implies that their experiments were probably skewed to larger clusters as the smaller clusters will likely have decayed by thermionic emission. Regardless, the key point here is that the statistical electron emission used in the current discussion has only one channel, whose contribution is diminishing as n increases and therefore will have its limitation in going to large clusters. Indeed, we already see that the contrast in the ratio for the π_3^* resonance in figure 4 is clearly becoming worse as n increases.

3.3. Photoelectron shifts arising from autodetachment

A second probe of resonances is through changes in the photoelectron spectra arising from different Franck–Condon factors associated with the π_1^* to neutral and the π_3^* to neutral state transitions, or from nuclear dynamics taking place on the π_3^* resonance [19]. Such electron loss channels (from a resonance)

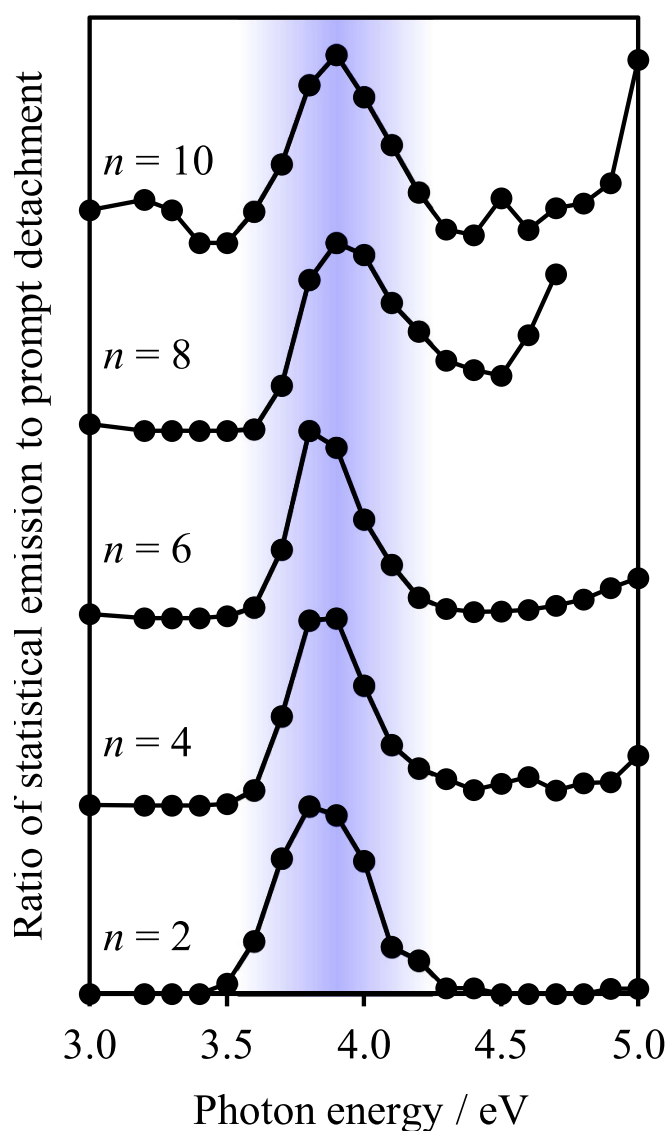


Figure 4. Ratio of statistical photoelectron emission to prompt photoelectron emission (see figure 3) for a range of cluster sizes, n . The data are plotted as arbitrary units and offset for clarity. The blue shaded area indicates the range over which the π_3^* resonance is excited.

are referred to as autodetachment. For $\text{U}^-(\text{H}_2\text{O})_2$, figure 5(a) shows the central peak position of the direct detachment feature to S_0 (i.e. the lower diagonal peak in figure 2(a)). The peak eKE, determined by fitting the direct detachment peak to a Gaussian function and taking the centre, shifts linearly to larger values as $h\nu$ increases. However, at the location of the π_3^* resonance, a clear deviation from this linear behaviour can be seen—the peak eKE is lower than expected in proximity of the π_3^* resonance, i.e. for $h\nu \approx 3.9$ eV. This shift to lower energy is consistent with the picture of autodetachment following some nuclear dynamics, where geometrical changes are driven by the potential gradient on the π_3^* state, reducing the energy gap between the resonance and S_0 neutral ground state. To illustrate further, the peak eKE as a function of $h\nu$ is fit to a linear function (with unit gradient) and figure 5(b) shows

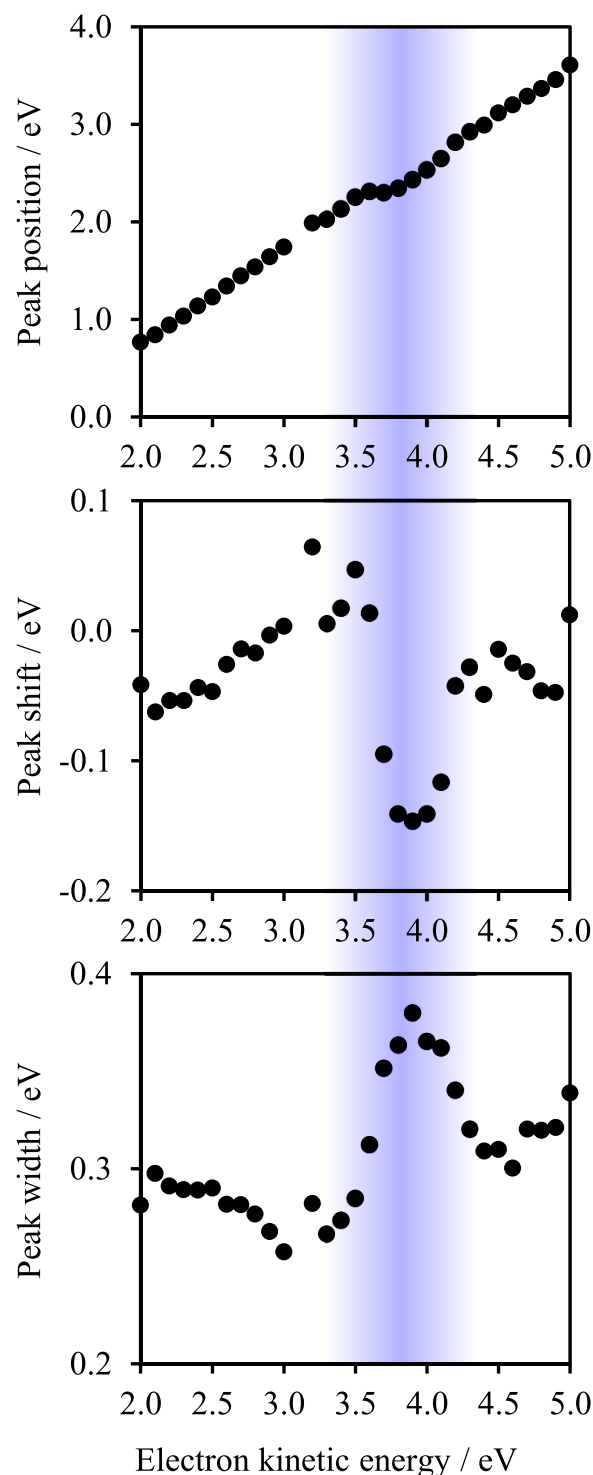


Figure 5. Determination of the resonance location based on the spectral changes in the prompt detachment peak (figure 3). (a) Central electron kinetic energy of peak as a function of photon energy. (b) Difference in peak position relative to expected position for a direct detachment process. (c) Spectral width of prompt detachment peak. The blue shaded area indicates the range over which the π_3^* resonance is excited.

the corresponding residuals. This variation of the peak eKE from the expected value for a direct detachment process clearly shows the location of the resonance. Finally, in figure 5(c), we

Table 1. Peak positions, $h\nu_{\max}$, and spectral widths, σ , determined from the ratio of statistically emitted electrons to promptly emitted electrons and determined from the deviation arising from autodetachment. All values are given in eV and the errors from Gaussian fits to determine $h\nu_{\max}$ do not exceed ± 0.02 eV.

n	Statistical emission		Autodetachment	
	$h\nu_{\max}$	σ	$h\nu_{\max}$	σ
2	3.91	0.23	3.94	0.33
3	3.88	0.15	4.01	0.28
4	3.87	0.13	4.01	0.26
6	3.86	0.12	4.01	0.23
8	4.02	0.20	4.04	0.30
10	3.90	0.15	4.03	0.27

show the spectral width associated with the high kinetic energy peak (based on the Gaussian fit). This similarly shows that, as the π_3^* resonance is accessed, the peak broadens due to the changing Franck–Condon factors and/or dynamics.

The position of the π_3^* resonance in figures 5(b) and (c) compares well to that in figure 4. Table 1 shows the peak positions determined from the two methods by fitting a Gaussian to the π_3^* resonance. Also included are the widths of the peaks. We conclude that, even though the ‘action’ used in either case is very different, the consistent results indicated that it is only the excitation of the π_3^* resonance that is important. Nevertheless, there are some differences. Specifically, π_3^* resonance position determined from the spectral deviation is on average 0.10 eV higher than that determined by the ratio of statistical to prompt detachment. This observed blue shift is likely associated with the inherent process leading to the observed action. The shift in the peak position arises from autodetachment that leads to changes in the Franck–Condon factors. These changes may be expected to be smaller at lower energy and increase with larger amounts of energy imparted by photoexcitation of the resonances. That is to say, the ‘true’ resonance position is likely closer to the onset of where the autodetachment feature is seen rather than the photon energy where the shift is the greatest, consistent with the observed data in table 1. Note also that the spectral width of the π_3^* resonance is 70% larger when determined using autodetachment as the action, suggesting that this method may be more sensitive to excitation to the π_3^* resonance than the ratio method.

In principle, the spectral deviation or spectral width methods described in this section do not suffer from the problems associated with not measuring the statistical electron emission. However, in going to larger clusters, the contrast in using the peak eKE shift also diminishes as does the width variation. These observations are likely a consequence of the fact that (i) the signal to noise is deteriorating as the initial ion currents are generally lower for larger clusters and (ii) the direct detachment peaks are becoming broader at larger n (which we return to below), which means that shifts and broadening are not as pronounced. Overall, the differing methods are complementary. However, for the π_2^* resonance, we found it much more challenging to perform any other method than the ratio of thermionic to direct detachment [28] because the photoelectron

spectra were poorly defined (see figure 2) and because many of the spectra were close to threshold so that distinguishing various contributions was complicated.

3.4. Photoelectron angular distributions

Finally, we also consider photoelectron angular distributions. Figure 2(b) shows that the anisotropy associated with the direct detachment peak in $U^-(H_2O)_2$ is largely negative ($\beta_2 < 0$), pointing to an emission predominantly perpendicular to the polarisation axis. Such behaviour is expected for photoelectron emission from a π orbital [47, 54] and therefore is consistent with the ground electronic state of the $U^-(H_2O)_2$ being the π_1^* state. In figure 6, the β_2 values averaged over the peak of the direct detachment feature are shown as a function of $h\nu$. Slow variations are expected. In figure 6, β_2 is becoming more negative as the π_3^* resonance ($h\nu = 3.9$ eV) is approached from the low energy side (note that at $h\nu \lesssim 2.7$ eV, the π_2^* resonance may also be participating). Near the position of the π_3^* resonance, sudden variations can be seen. For $n = 2$, there is a clear ‘kink’ with the gradient changing sign suddenly. These variations are also clearly discernible for $n = 4$ and 6, but less so for $n \geq 8$. Taking differences from the expected value (as done in the preceding section for the photoelectron peak positions) does not offer provide better contrast because the variations are small and because the scatter associated with adjacent data points is relatively large (especially for the larger clusters).

The action in the present case is a change in the β_2 values. In some cases, such changes are dramatic and easily observed [24, 50, 55–57]. In the present case on the other hand, the variations are small and therefore difficult to discern. This may be because all the resonances are of very similar character and the system has no symmetry. For example, in anthracene or pyrene, even though the resonances are also of π^* character, their associated β_2 values upon emission varied dramatically for some (but not all) resonances [20, 21]. Unfortunately, the theory to quantitatively predict these changes has not yet been developed. Nevertheless, in the case of $U^-(H_2O)_n$ for the π_3^* resonance, it does not appear that photoelectron angular distributions are particularly sensitive. Although changes in the anisotropy of the direct detachment feature across the resonance were very small, electrons being lost through autodetachment appear to be ejected with a more negative β_2 value. Again, as the resonances of $U^-(H_2O)_n$ are also π^* character, the anisotropy change in going from direct detachment to autodetachment is not as pronounced as it could be for other molecules.

Considering the application of photoelectron angular distributions to larger clusters might also be complicated. In figures 7(a) and (b), the photoelectron spectra and β_2 values are shown for photoelectron spectra taken at $h\nu = 3.6$ eV (i.e. off-resonance) across a wide range of n (up to $n = 25$). From this, it is apparent that the β_2 values are becoming more isotropic for larger clusters. This is in part because the eKE is smaller [58] as shown in the corresponding photoelectron spectra, but also contains scattering contributions of the outgoing electron by the water molecules leading to a tendency

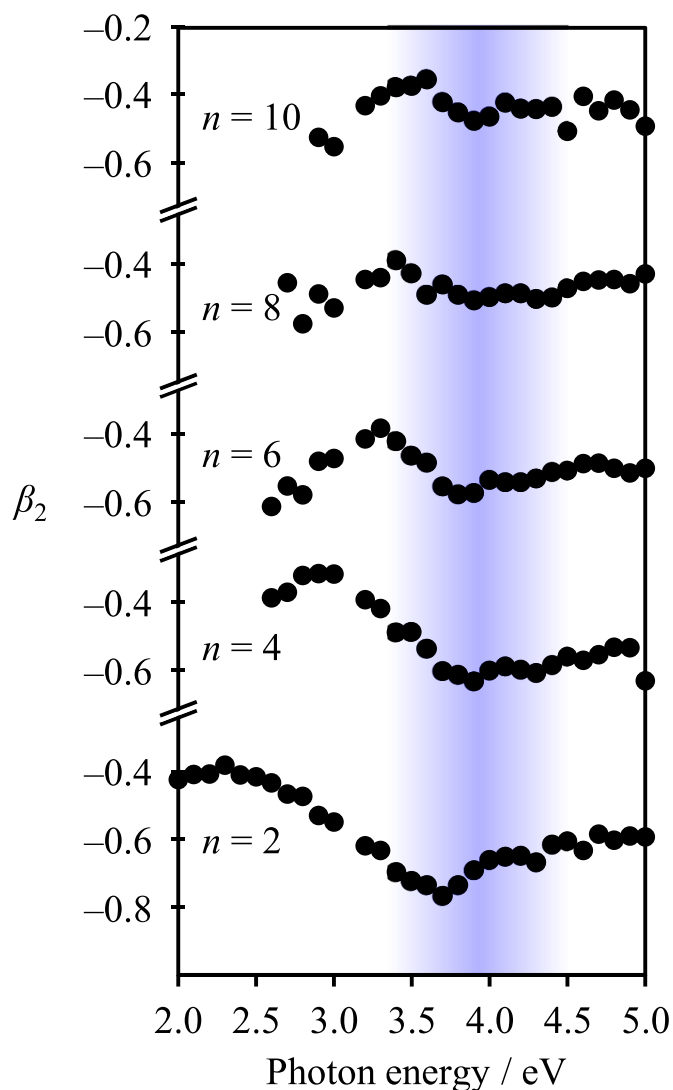


Figure 6. β_2 characterising the photoelectron angular distribution of the prompt photoelectron emission for a range of cluster sizes, n . The blue shaded area indicates the range over which the π_3^* resonance is excited.

to isotropic photoelectron angular distributions, as shown in water clusters by Hartweg *et al* [59]. Hence, while photoelectron angular distributions may be useful for identifying electronic resonances in isolated species, they are likely not to be useful in large clusters. This can already be appreciated from the data in figure 6 for $n \geq 8$.

4. Direct detachment in larger clusters and analysis of reorganisation energy

In the preceding section, we focussed on the identification of shape resonances in $U^-(H_2O)_n$ and specifically the π_3^* resonance. A key conclusion from our previous work on water clusters of a series of polycyclic aromatic hydrocarbon radical anions, PAH^- , was that the position of resonances does not change dramatically with respect to the anion ground state (i.e. excitation energy in the anion photoelectron spectroscopy

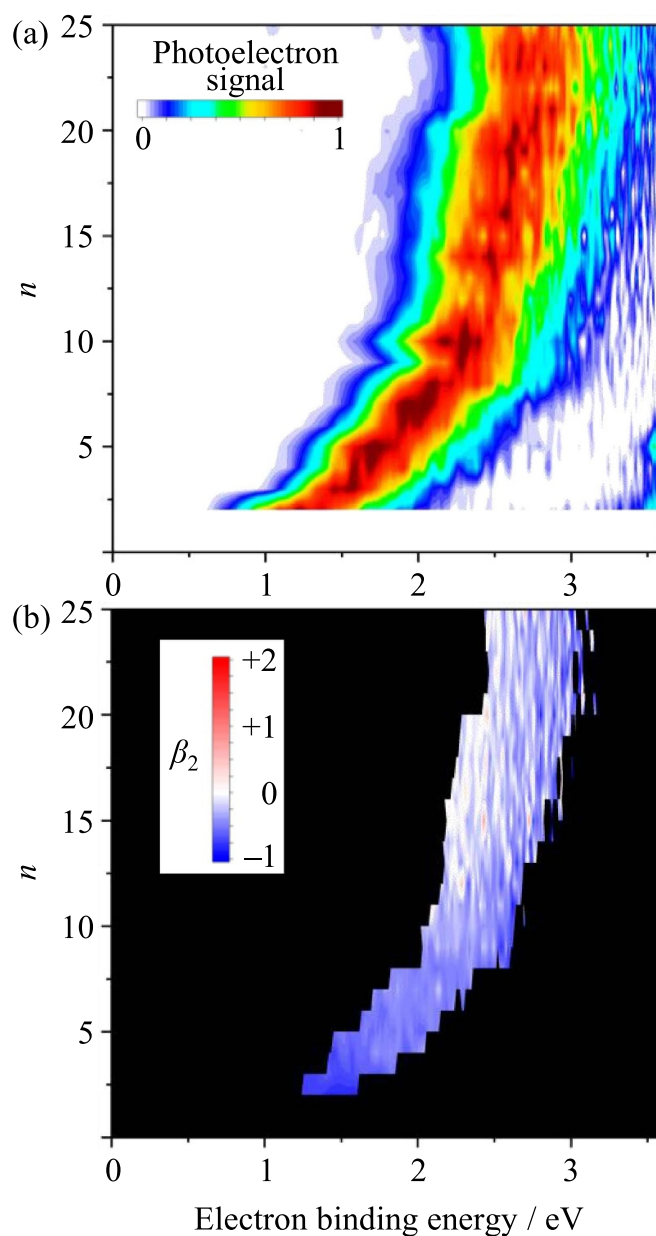


Figure 7. (a) Photoelectron spectra acquired at $h\nu = 3.6$ eV plotted in terms of binding energy for a range of cluster sizes from $n = 2$ to $n = 25$. The peak maximum corresponds to the vertical detachment energy whilst the peak onset corresponds to the adiabatic detachment energy. (b) Anisotropy parameters associated with the photoelectron spectra in (a). The blacked out area corresponds to areas where the photoelectron signal is less than 50% of its maximum.

experiments) [26, 27]. The same holds for $U^-(H_2O)_n$ [28]. However, this constant excitation energy is of course relative to the anion ground state and we know from figure 7(a) that the anion ground state is becoming more bound with increasing n . Therefore, when referencing an energy level diagram with respect to the neutral ground state, the resonances are decreasing in energy [26, 28]. In figure 8, we show the results from our previous study extending the energies derived from the photoelectron spectra (figure 7(a)) and the resonance positions to infinite cluster size. The data are shown as a function

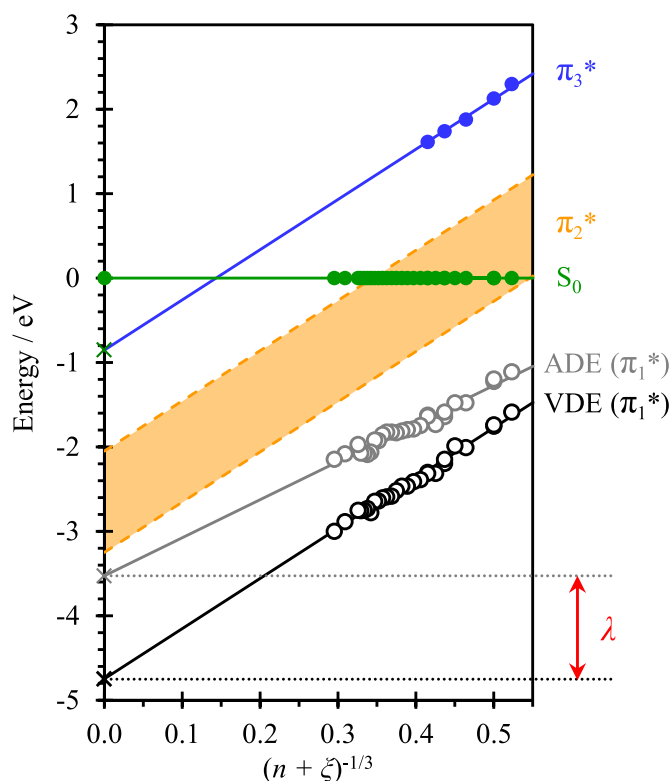


Figure 8. Energy level diagram for $U^-(H_2O)_n$ clusters, relative to the ground state of the neutral cluster, S_0 , plotted as a function of cluster size, $(n + \xi)^{-1/3}$. Circles are taken from photoelectron spectra and represent the anion ground state π_1^* and the π_3^* resonance, and the dashed lines represent the extracted range of the π_2^* resonance. Linear fits (considering $n \geq 3$) to the vertical and adiabatic detachment energy are extended to their respective bulk aqueous limits, shown with crosses. The difference between these extrapolated energies corresponds to the reorganization energy, λ . Adapted from [28]. CC BY 4.0.

of $(n + \xi)^{-1/3}$, which effectively corresponds to a cluster size in which ξ is the volume taken up by the solute ion (U^- in the present case) in terms of equivalent water molecules [60, 61]. We have taken $\xi = 4$ based on a consideration of the experimental and computed partial molar volume of aqueous U , and on dielectric continuum theory [28, 62, 63].

The extrapolation in figure 8 shows that several electronic states which are resonances in the isolated molecule may become bound in larger clusters and the bulk. However, while our photoelectron spectroscopy measurements allow for mass-selection so that the linear extrapolation with cluster size can be deployed to determine bulk properties, these bulk properties are in the reference frame of the anion. Instead, if one seeks to understand electron attachment processes and resonances in bulk aqueous environments, then the desired reference frame is that of the neutral geometry, to which an electron is attached (i.e. a vertical electron attachment energy).

The electron detachment and electron attachment pictures can be connected through a Marcus-type picture [28, 30]. Assuming a linear response, the energy curves along combined intra-molecular (inner-sphere) and inter-molecular (outer-sphere) coordinates then scale parabolically and one can

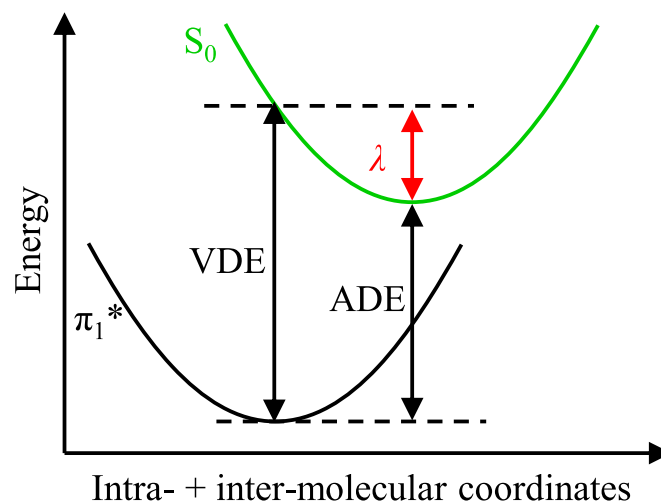


Figure 9. Schematic of energy curves within a linear response model along the intramolecular and intermolecular coordinates linking $U^-(H_2O)_n$ (black) and $U(H_2O)_n$ (green). The experimental observables of the vertical detachment energy (VDE) and adiabatic detachment energy (ADE) are shown as vertical double arrows along with their difference which corresponds to the reorganisation energy (λ). The vertical attachment energy to specific resonances (not shown in figure) is then the vertical excitation energy of the resonance in the anion geometry minus the VDE plus twice λ . These quantities can be determined for different n and in the limit of $n \rightarrow \infty$ (figure 8).

define the reorganisation energy, λ , as shown in figure 9. The value of λ can be estimated from the non-resonant photoelectron spectra: according to figure 9, λ equates to the difference between the vertical detachment energy and the adiabatic detachment energy (the electron affinity). These can be obtained directly from figure 8 which finds that $\lambda \sim 1.2$ eV in the bulk limit. This reorganisation energy contains both the intramolecular reorganisation, λ_{IS} , associated with the geometry change of U in going from anion to neutral, and the intermolecular reorganisation, λ_{OS} , associated with overall change in solvation sphere between anionic and neutral U . In the case of $PAH^-(H_2O)_n$, λ_{IS} is small because the geometry change upon the addition of an electron to a PAH such as anthracene or pyrene is minor [20, 64]. In contrast, for $U^-(H_2O)_n$, there is a large change in geometry as evidenced by the broadness of the photoelectron spectrum of the direct detachment. At first glance, this could be viewed as invalidating our approach of using photoelectron spectroscopy as a probe of electron-impact resonances, but in actuality, it offers direct insight into λ_{IS} , under the assumption that the motion connecting the two geometries is harmonic. In addition to the intramolecular changes, it is also clear that the direct photoelectron spectra are increasing in spectral width as shown in figure 7(a), which is associated with the solvent response rather than the intramolecular changes. We now consider the decomposition of the total λ into the individual contributions, $\lambda = \lambda_{IS} + \lambda_{OS}$.

The core problem in determining λ_{IS} is that the lowest lying valence state of U is a resonance [10]. Hence, we cannot simply measure the photoelectron spectrum of U^- in its π_1^* state. However, a single water molecule renders the π_1^* state

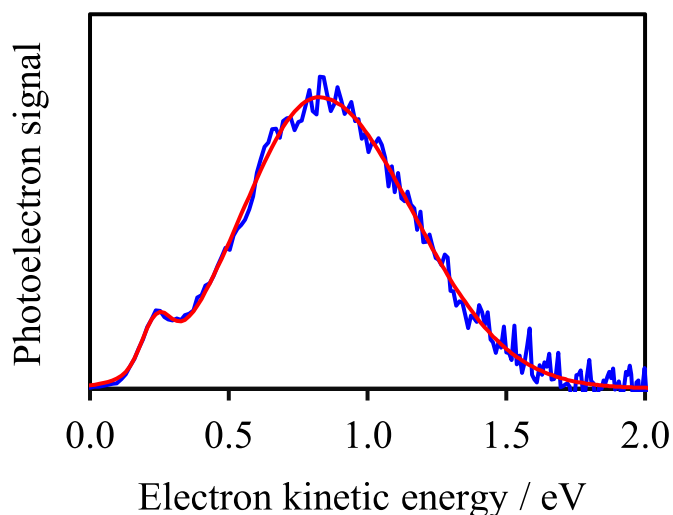


Figure 10. Photoelectron spectrum of $\text{U}^-(\text{H}_2\text{O})_1$ (blue), together with a fit to the experimental data (red), which allows us to estimate the intramolecular reorganisation energy as $\lambda_{\text{IS}} = \text{VDE} - \text{ADE} \sim 0.6 \text{ eV}$.

as the ground state and will have a minimal intermolecular reorganisation effect. In figure 10, the photoelectron spectrum of $\text{U}^-(\text{H}_2\text{O})_1$ is presented. This spectrum shows a relatively narrow peak at low binding energy and a broader peak at higher binding energy. The former is consistent with the detachment from a dipole-bound state whilst the latter with detachment from a valence-bound state, which in this case is the π_1^* state. The observation of both types of electronic states indicates that there is a distribution of isomers in the molecular beam. A similar observation was made by Bowen and coworkers for the case of $\text{U}^-(\text{Xe})_1$ [37], but they only observed the valence-bound isomer for $\text{U}^-(\text{H}_2\text{O})_1$ [37, 38]. Computational work has suggested that differing locations of the H_2O molecule leads to differing binding energies of the valence state [65]. Hence, the differing isomers might reflect different structural isomers. Only one isomer, however, was found to have the valence state as the lowest energy electronic structure [65]. We fit this photoelectron spectrum with a Gaussian function to represent the dipole-bound state and an asymmetric Gaussian for the π_1^* state, as shown in figure 10. From the fits, we determine that the adiabatic detachment energy is 0.25 eV and the vertical detachment energy is 0.85 eV, consistent with previous experiments. Taken together, their difference therefore is a reasonable measure of λ_{IS} and we find that $\lambda_{\text{IS}} \sim 0.6 \text{ eV}$.

The total reorganisation energy is $\lambda \sim 1.2 \text{ eV}$, from extrapolation of the adiabatic and vertical detachment energies of the clusters to infinite size. But given that $\lambda = \lambda_{\text{IS}} + \lambda_{\text{OS}}$, we determine that $\lambda_{\text{OS}} \sim 0.6 \text{ eV}$ in aqueous solution. Hence, there is an approximately equal contribution to the reorganisation energy from the change in geometry of the solute and from the solvent. The contribution of λ_{OS} will be dependent on n , which is consistent with the diverging extrapolations of the adiabatic and vertical detachment energies discussed previously. Elegantly, our cluster approach allows the total reorganisation

energy to be deconvoluted into its separate contributions. These values should also serve as a useful benchmark for computational work aimed at understanding electronic resonances in bulk aqueous environments [66–70].

5. Conclusions

Anionic clusters offer a route of measuring electronic resonances in micro-solvated environments by using 2D photoelectron spectroscopy to access the resonances. Several methods for extracting the resonance positions have been outlined. Anisotropy in the photoelectron angular distribution responds to the photon energy scanning over a resonance, although this may only be usefully distinguishable when the character of the excited state differs greatly to the ground state. The most sensitive method appears to be the use of statistical emission relative to direct detachment, although this requires that such emission can be measured which is not guaranteed, especially as the cluster size increases. This would be complementary to other action spectroscopies that have not been considered here. For example, ion-yield spectra probing the depletion of the parent $\text{U}^-(\text{H}_2\text{O})_n$ signal would also yield the position of the resonance(s), but would be blind to the electron loss channel that was the focus here. Nevertheless, our previous conclusion that excitation energies to the resonances from the anion do not change significantly with cluster size appears to hold, even for strong interactions between solute and solvent.

2D photoelectron spectroscopy probes the resonances from the perspective of the anion, whilst the inherent interest is in electronic resonances that can capture free electrons which requires a neutral initial geometry. By considering the adiabatic and vertical detachment energies, the reorganisation energy can be determined. Moreover, as shown here, this can be deconvoluted into its intramolecular and intermolecular contributions. In the specific case of aqueous uracil, we find that the former amounts to $\sim 0.6 \text{ eV}$ while the latter to $\sim 0.6 \text{ eV}$ of the total $\sim 1.2 \text{ eV}$ reorganisation energy in the bulk. Taken holistically, photoelectron spectroscopy studies on anionic water clusters offer a new and elegant route to probing electronic resonances in aqueous environments.

Data availability statement

All data that support the findings of this study are included within the article (and any supplementary files).

Acknowledgments

This work was supported by the EPSRC under Grant EP/V007971/1. Connor Clarke was supported by the Durham Doctoral Scholarship scheme.

ORCID iDs

Connor J Clarke  <https://orcid.org/0000-0001-8825-3149>
Jan R R Verlet  <https://orcid.org/0000-0002-9480-432X>

References

- [1] Garrett B C *et al* 2005 Role of water in electron-initiated processes and radical chemistry: issues and scientific advances *Chem. Rev.* **105** 355–90
- [2] Alizadeh E and Sanche L 2012 Precursors of solvated electrons in radiobiological physics and chemistry *Chem. Rev.* **112** 5578–602
- [3] Gao Y, Zheng Y and Sanche L 2021 Low-energy electron damage to condensed-phase DNA and its constituents *Int. J. Mol. Sci.* **22** 7879
- [4] Gorfinkiel J D and Ptasińska S 2017 Electron scattering from molecules and molecular aggregates of biological relevance *J. Phys. B: At. Mol. Opt. Phys.* **50** 182001
- [5] Ingólfsson O 2019 *Low-Energy Electrons: Fundamentals and Applications* (CRC Press)
- [6] Gorfinkiel J D 2020 Electron collisions with molecules and molecular clusters *Eur. Phys. J. D* **74** 51
- [7] Boudäiffa B, Cloutier P, Hunting D, Huels M A and Sanche L 2000 Resonant formation of DNA strand breaks by low-energy (3–20 eV) electrons *Science* **287** 1658–60
- [8] Martin F, Burrow P D, Cai Z, Cloutier P, Hunting D and Sanche L 2004 DNA strand breaks induced by 0–4 eV electrons: the role of shape resonances *Phys. Rev. Lett.* **93** 068101
- [9] Simons J 2006 How do low-energy (0.1–2 eV) electrons cause DNA-strand breaks? *Acc. Chem. Res.* **39** 772–9
- [10] Afatooni K, Gallup G A and Burrow P D 1998 Electron attachment energies of the DNA bases *J. Phys. Chem. A* **102** 6205–7
- [11] Desfrancois C, Abdoul-Carime H and Schermann J P 1996 Electron attachment to isolated nucleic acid bases *J. Chem. Phys.* **104** 7792–4
- [12] Hanel G, Gstir B, Denifl S, Scheier P, Probst M, Farizon B, Farizon M, Illenberger E and Märk T D 2003 Electron attachment to uracil: effective destruction at subexcitation energies *Phys. Rev. Lett.* **90** 188104
- [13] Denifl S, Ptasińska S, Hanel G, Gstir B, Probst M, Scheier P and Märk T D 2004 Electron attachment to gas-phase uracil *J. Chem. Phys.* **120** 6557–65
- [14] Ptasińska S, Denifl S, Scheier P, Illenberger E and Märk T D 2005 Bond- and site-selective loss of H atoms from nucleobases by very-low-energy electrons (<3 eV) *Angew. Chem., Int. Ed.* **44** 6941–3
- [15] Burrow P D, Gallup G A, Scheer A M, Denifl S, Ptasińska S, Märk T and Scheier P 2006 Vibrational Feshbach resonances in uracil and thymine *J. Chem. Phys.* **124** 124310
- [16] da Silva F F *et al* 2013 NCO^- , a key fragment upon dissociative electron attachment and electron transfer to pyrimidine bases: site selectivity for a slow decay process *J. Am. Soc. Mass Spectrom.* **24** 1787–97
- [17] Kočišek J, Pysanenko A, Fárnik M and Fedor J 2016 Microhydration prevents fragmentation of uracil and thymine by low-energy electrons *J. Phys. Chem. Lett.* **7** 3401–5
- [18] West C W, Bull J N, Antonkov E and Verlet J R R 2014 Anion resonances of para-benzoquinone probed by frequency-resolved photoelectron imaging *J. Phys. Chem. A* **118** 11346–54
- [19] Anstöter C S, Bull J N and Verlet J R R 2016 Ultrafast dynamics of temporary anions probed through the prism of photodetachment *Int. Rev. Phys. Chem.* **35** 509–38
- [20] Mensa-Bonsu G, Lietard A, Tozer D J and Verlet J R R 2020 Low energy electron impact resonances of anthracene probed by 2D photoelectron imaging of its radical anion *J. Chem. Phys.* **152** 174303
- [21] Lietard A, Verlet J R R, Slimak S and Jordan K D 2021 Temporary anion resonances of pyrene: a 2D photoelectron imaging and computational study *J. Phys. Chem. A* **125** 7004–13
- [22] Horke D A, Li Q, Blancafort L and Verlet J R R 2013 Ultrafast above-threshold dynamics of the radical anion of a prototypical quinone electron-acceptor *Nat. Chem.* **5** 711–7
- [23] Bull J N, West C W and Verlet J R R 2015 On the formation of anions: frequency-, angle-, and time-resolved photoelectron imaging of the menadione radical anion *Chem. Sci.* **6** 1578–89
- [24] West C W, Bull J N, Hudson A S, Cobb S L and Verlet J R R 2015 Excited state dynamics of the isolated green fluorescent protein chromophore anion following UV excitation *J. Phys. Chem. B* **119** 3982–7
- [25] Mensa-Bonsu G, Lietard A and Verlet J R R 2019 Enhancement of electron accepting ability of para-benzoquinone by a single water molecule *Phys. Chem. Chem. Phys.* **21** 21689–92
- [26] Lietard A, Mensa-Bonsu G and Verlet J R R 2021 The effect of solvation on electron capture revealed using anion two-dimensional photoelectron spectroscopy *Nat. Chem.* **13** 737
- [27] Lietard A and Verlet J R R 2022 Effect of microhydration on the temporary anion states of pyrene *J. Phys. Chem. Lett.* **13** 3529–33
- [28] Cooper G A, Clarke C J and Verlet J R R 2023 Low-energy shape resonances of a nucleobase in water *J. Am. Chem. Soc.* **145** 1319–26
- [29] Marcus R A 1956 On the theory of oxidation-reduction reactions involving electron transfer. I *J. Chem. Phys.* **24** 966–78
- [30] Marcus R A 1964 Chemical and electrochemical electron-transfer theory *Annu. Rev. Phys. Chem.* **15** 155–96
- [31] Wiley W C and McLaren I H 1955 Time-of-flight mass spectrometer with improved resolution *Rev. Sci. Instrum.* **26** 1150–7
- [32] Eppink A T J B and Parker D H 1997 Velocity map imaging of ions and electrons using electrostatic lenses: application in photoelectron and photofragment ion imaging of molecular oxygen *Rev. Sci. Instrum.* **68** 3477–84
- [33] Horke D A, Roberts G M, Lecointre J and Verlet J R R 2012 Velocity-map imaging at low extraction fields *Rev. Sci. Instrum.* **83** 063101
- [34] Rogers J P, Anstöter C S, Bull J N, Curchod B F E and Verlet J R R 2019 Photoelectron spectroscopy of the hexafluorobenzene cluster anions: $(\text{C}_6\text{F}_6)_n^-$ ($n = 1-5$) and $\Gamma^-(\text{C}_6\text{F}_6)$ *J. Phys. Chem. A* **123** 1602–12
- [35] Even U 2015 The Even-Lavie valve as a source for high intensity supersonic beam *EPJ Tech. Instrum.* **2** 1–22
- [36] Roberts G M, Nixon J L, Lecointre J, Wrede E and Verlet J R R 2009 Toward real-time charged-particle image reconstruction using polar onion-peeling *Rev. Sci. Instrum.* **80** 053104
- [37] Hendricks J H, Lyapustina S A, de Clercq H L and Bowen K H 1998 The dipole bound-to-covalent anion transformation in uracil *J. Chem. Phys.* **108** 8–11
- [38] Schiedt J, Weinkauff R, Neumark D M and Schlag E W 1998 Anion spectroscopy of uracil, thymine and the amino-oxo and amino-hydroxy tautomers of cytosine and their water clusters *Chem. Phys.* **239** 511–24
- [39] Campbell E E B and Levine R D 2000 Delayed ionization and fragmentation en route to thermionic emission: statistics and dynamics *Annu. Rev. Phys. Chem.* **51** 65–98
- [40] Andersen J U, Bonderup E and Hansen K 2002 Thermionic emission from clusters *J. Phys. B: At. Mol. Opt. Phys.* **35** R1
- [41] Adams C L, Hansen K and Weber J M 2019 Vibrational autodetachment from anionic nitroalkane chains: from molecular signatures to thermionic emission *J. Phys. Chem. A* **123** 8562–70

- [42] West C W, Hudson A S, Cobb S L and Verlet J R R 2013 Communication: autodetachment versus internal conversion from the S_1 state of the isolated GFP chromophore anion *J. Chem. Phys.* **139** 071104
- [43] Jalehdoust A and von Issendorff B 2023 Photon energy dependence of the photoelectron spectra of the anthracene anion: on the influence of autodetaching states *J. Chem. Phys.* **158** 194302
- [44] Regeta K and Allan M 2013 Autodetachment dynamics of acrylonitrile anion revealed by two-dimensional electron impact spectra *Phys. Rev. Lett.* **110** 203201
- [45] Anstötter C S, Mensa-Bonsu G, Nag P, Ranković M, Kumar T, Boichenko R, N A, Bochenkova A V, Fedor J and Verlet J R R 2020 Mode-specific vibrational autodetachment following excitation of electronic resonances by electrons and photons *Phys. Rev. Lett.* **124** 203401
- [46] Reid K L 2003 Photoelectron angular distributions *Annu. Rev. Phys. Chem.* **54** 397–424
- [47] Sanov A 2014 Laboratory-frame photoelectron angular distributions in anion photodetachment: insight into electronic structure and intermolecular interactions *Annu. Rev. Phys. Chem.* **65** 341–63
- [48] Cooper J and Zare R N 1968 Angular distribution of photoelectrons *J. Chem. Phys.* **48** 942–3
- [49] Bull J N, West C W and Verlet J R R 2015 Anion resonances and above-threshold dynamics of coenzyme Q0 *Phys. Chem. Chem. Phys.* **17** 16125–35
- [50] Anstötter C S, Dean C R and Verlet J R R 2017 Chromophores of chromophores: a bottom-up Hückel picture of the excited states of photoactive proteins *Phys. Chem. Chem. Phys.* **19** 29772–9
- [51] Bull J N and Verlet J R R 2017 Dynamics of Π^* -resonances in anionic clusters of para-toluquinone *Phys. Chem. Chem. Phys.* **19** 26589–95
- [52] Bull J N, West C W and Verlet J R R 2016 Ultrafast dynamics of formation and autodetachment of a dipole-bound state in an open-shell π -stacked dimer anion *Chem. Sci.* **7** 5352–61
- [53] Markovich G, Pollack S, Giniger R and Cheshnovsky O 1994 Photoelectron spectroscopy of Cl^- , Br^- , and I^- solvated in water clusters *J. Chem. Phys.* **101** 9344–53
- [54] Anstötter C S and Verlet J R R 2021 Modeling the photoelectron angular distributions of molecular anions: roles of the basis set, orbital choice, and geometry *J. Phys. Chem. A* **125** 4888–95
- [55] Jagau T-C, Dao D B, Holtgrewe N S, Krylov A I and Mabbs R 2015 Same but different: dipole-stabilized shape resonances in CuF^- and AgF^- *J. Phys. Chem. Lett.* **6** 2786–93
- [56] Stanley L H, Anstötter C S and Verlet J R R 2017 Resonances of the anthracenyl anion probed by frequency-resolved photoelectron imaging of collision-induced dissociated anthracene carboxylic acid *Chem. Sci.* **8** 3054–61
- [57] Anstötter C S and Verlet J R R 2022 A Hückel model for the excited-state dynamics of a protein chromophore developed using photoelectron imaging *Acc. Chem. Res.* **55** 1205–13
- [58] Wigner E P 1948 On the behavior of cross sections near thresholds *Phys. Rev.* **73** 1002–9
- [59] Hartweg S, Yoder B L, Garcia G A, Nahon L and Signorell R 2017 Size-resolved photoelectron anisotropy of gas phase water clusters and predictions for liquid water *Phys. Rev. Lett.* **118** 103402
- [60] Jortner J 1992 Cluster size effects *Z. Phys. D* **24** 247–75
- [61] Coe J V 1997 Connecting cluster anion properties to bulk: ion solvation free energy trends with cluster size and the surface vs internal nature of iodide in water clusters *J. Phys. Chem. A* **101** 2055–63
- [62] Fucaloro A F, Dewey K, Fan G, Imuta K, Jensen D and Muranaka M 2008 Partial molar volumes of uracil, thymine, adenine in water and of adenine in aqueous solutions of uracil and thymine *J. Solut. Chem.* **37** 1289–304
- [63] Lowe A R, Cox J S and Tremaine P R 2017 Thermodynamics of aqueous adenine: standard partial molar volumes and heat capacities of adenine, adeninium chloride, and sodium adeninate from $T=283.15\text{K}$ to 363.15K *J. Chem. Thermodyn.* **112** 129–45
- [64] Kregel S J, Thurston G K and Garand E 2018 Photoelectron spectroscopy of anthracene and fluoranthene radical anions *J. Chem. Phys.* **148** 234306
- [65] Anstötter C S and Matsika S 2020 Understanding the interplay between the nonvalence and valence states of the uracil anion upon monohydration *J. Phys. Chem. A* **124** 9237–43
- [66] Sieradzka A and Gorfinkiel J D 2017 Theoretical study of resonance formation in microhydrated molecules. II. Thymine-(H_2O) $_n$, $n = 1, 2, 3, 5$ *J. Chem. Phys.* **147** 034303
- [67] Sieradzka A and Gorfinkiel J D 2017 Theoretical study of resonance formation in microhydrated molecules. I. Pyridine-(H_2O) $_n$, $n = 1, 2, 3, 5$ *J. Chem. Phys.* **147** 034302
- [68] Mukherjee M, Tripathi D, Brehm M, Riplinger C and Dutta A K 2021 Efficient EOM-CC-based protocol for the calculation of electron affinity of solvated nucleobases: uracil as a case study *J. Chem. Theory Comput.* **17** 105–16
- [69] Anstötter C S, DelloStritto M, Klein M L and Matsika S 2021 Modeling the ultrafast electron attachment dynamics of solvated uracil *J. Phys. Chem. A* **125** 6995–7003
- [70] Verma P, Ghosh D and Dutta A K 2021 Electron attachment to cytosine: the role of water *J. Phys. Chem. A* **125** 4683–94